Building a Quantum-Enabled, Networked Radar Testbed for Urban Surveillance of Low Observable Aerial Targets – Current Status

Mohammed Jahangir[1], Darren Griffiths[2], Yeshpal Singh[3] and Michail Antoniou[4]

University of Birmingham
Edgbaston, Birmingham
UNITED KINGDOM

{[1]m.jahangir, [2]dxg066, [3]y.singh.1, [4]m.antoniou}@bham.ac.uk,

ABSTRACT

The University of Birmingham (UoB) are investigating the potential benefits of frequency locking radar networks using a Quantum frequency source, with Phase Noise (PN) several orders of magnitude lower (at low frequency offsets) than what is available using commercially available oscillator technology. To understand the utility of quantum oscillators in radar systems and to identify its potential and challenges through practical demonstration and under demanding realistic conditions, we are developing a full-scale, quantum-enabled radar facility. The facility consists of two COTS L-band staring radars installed at UoB campus, to demonstrate the capability of highly stable ultra-low PN oscillators we possess, for improving radar sensitivity and network synchronisation. The facility is generic and in its final form can be over-arching in terms of its application, however, as the starting point we are considering radar detection of low observable targets such as drones in an urban setting. Those can present significant challenges as the inherent imperfections in local oscillators introduces PN that results in strong clutter masking weak target echoes, thus forming a representative scenario where the strength of quantum oscillators can be assessed.

The paper summarises the current status of the development of the facility. Baseline performance for the networked radar is reported using real measurements from a challenging urban environment. In parallel, bench tests have been carried out on the optical oscillators and the PN and Allan deviation has been compared with those of the conventional OCXO oscillators used in the current radar. Finally, the measurement plan is outlined for the phased introduction of an external reference source to the radar testbed which will be used to evaluate the photonic/quantum oscillators.

1.0 INTRODUCTION

Right from the early days of radar development, reducing system noise has been a key driver for hardware design. For example, great attention is paid to ensuring that there is a low amount of receiver noise so that faint echoes can be adequately detected. However, a fundamental limit in radar system sensitivity, especially in the detection of slow-moving targets, is Phase Noise (PN). Even in today's highly advanced radar systems, PN due to an imperfect local oscillator signal, can still act as a fundamental limit on system sensitivity in the presence of high and usually close-in clutter, exceeding that of receiver thermal noise and masking the presence of weak echoes. Quantum transitions have long been recognised for their inherent frequency/time stability and hence are an attractive technology for a wide range of timing applications.

At its heart, radar is a timing device whose accuracy will be determined by the purity of the oscillator signal used. At the University of Birmingham (UoB) novel, high performing, quantum oscillators are being married to advanced, all-digital, staring radar systems to examine their resulting performance. To fully exercise the capability of the quantum oscillators, both a traditional monostatic and a more complex multistatic configuration are assessed. To gain a comprehensive understanding of the change in performance that can be bought about by quantum oscillators, results are benchmarked against the existing conventional oven controlled crystal oscillator (OCXO) currently used in the staring radar. Staring radars have been selected as

their long integration times inherently require low PN and for very high clutter, clutter PN can exceed receiver noise. Multistatic staring radars have been chosen as it is well known that the degree of "self-cancellation" that occurs in monostatic radar is absent in a remote receiver, making coherency in a multistatic network harder to achieve. Again, performance will be benchmarked against an identical network but one that uses commercially available oscillators.

This paper describes the development of the quantum-enabled networked radar at UoB and reports on its current status. Section 2 provides a blue print for the photonics and Quantum oscillators as an alternative source for reference frequency for radar systems. Section 3 describes the networked staring radar testbed set-up within an urban environment and baseline performance results from real radar trials are reported in section 4. Section 5 compares the conventional oscillators with a variant of the alternative oscillator using data obtained from bench tests and future plans for validating the radar performance against the fully integrated oscillators are outlined in section 6. Finally, the overall summary is given in section 7.

2.0   High Fidelity Oscillators

The performance of any clock or frequency standard can be quantified by its instability (statistical fluctuations of the output frequency) and the uncertainty (how well the system realises the desired frequency), which are analogous to the typical examples of precision and accuracy, respectively. Both Figures of Merit (FoM) are measured in fractional frequency units, i.e., normalised by the output frequency. Optical clocks are able to achieve better performance than microwave clocks, in both FoM, due to the 10^5 factor increase in output frequency, as many of the perturbations and systematic effects are of similar size. In this work, the task of synthesising microwaves from the optical signal can be accomplished by a Menlo Microwave generator unit PWMG-1500 (Menlo) ([1], [2]). This system consists of an optical Frequency Comb (F-Comb) and an Optical Reference Source (ORS) which is an ultra-stable laser operating at 1542 nm. The F-Comb is a pulsed laser that is tightly locked to the ORS and down-converts the optical frequency to an RF frequency in a phase coherent manner, resulting in little degradation of the PN. Microwaves synthesised from high-quality optical reference demonstrate not only the unrivalled accuracy of optical clocks, but also lower PN than traditional microwave sources [3].

A further technological advancement is to operate the optical clock through locking the optical reference frequencies to a well-defined transition between two energy levels within a chosen atom. UoB is developing a cold atom based strontium optical lattice clock operating on the 698 nm intercombination line $^1S_0 \rightarrow {}^3P_0$ [4]. An ultra-stable laser at 698 nm (Clock Laser) can then be locked to the atomic transition via periodic Rabi spectroscopy. The cold atom based technique provides a frequency lock relatively slowly, with a servo bandwidth <1 Hz, thus the short-term performance of the system is dominated by the Clock Laser and its longer frequency stability is set by the strontium clock. Using telecommunication fibres to transfer the laser signal over a distance requires referencing the Clock Laser to a 1397 nm ultra-stable laser (Transfer Laser), suitable for transmission over the fibre network. The locking operation is performed via second harmonic generation and electronic feedback from the atom lock. However, the transmission of laser over a fibre link can cause PN degradation due to diurnal temperature effects and acoustic noise. These can be managed by actively stabilising the optical path length of the fibre. An interface node at the Menlo side will be designed to perform the fibre path length stabilisation and locks the F-Comb to the Transfer Laser signal in place of its internal ORS. This set-up will then result in a Quantum-enabled radar. For a network set-up a Menlo unit will be required at each radar node and linked up to the central strontium clock via the PN stabilised fibre network. Whilst the full architecture for the Quantum oscillator enabled radar is depicted in Figure 1, the initial effort has addressed understanding the oscillator characteristic of the Menlo and devising a testbed comprising a suitable radar system to evaluate the highly stable ultra-low PN oscillator for real radar applications.
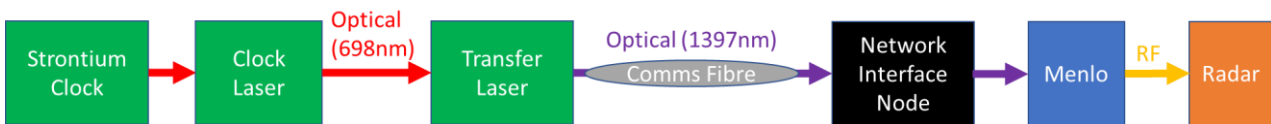
Figure 1: Schematic illustration of a quantum-enabled radar.

3.0 RADAR USE CASE

3.1 Radar Overview

Staring radars have attracted interest in recent years due to the advantages in the surveillance of small airborne targets such as drones [5]. They offer a convenient use case to test the radar performance limits with respect to system PN as their long integration times for processing small targets inherently require low PN and in situations of very strong clutter, clutter PN can exceed receiver noise.

An early prototype L-band staring system developed by Thales is selected as the reference radar system. It is detailed in [6] and uses a broad beam antenna on transmit and a 2-D array of receivers that are digitised at the element level. The receiver array has an angular coverage of 90° in azimuth and 60° in elevation. It is a ~2 MHz bandwidth pulse radar with ~8 kHz Pulse Repetition Frequency (PRF). There is a total of 64 receivers arranged in a 4 × 16 array providing the means to form simultaneous multiple beams on receive over its entire Field of Regard (FOR) (Figure 2) and therefore is able to maintain persistence dwell on all targets within its FOV.
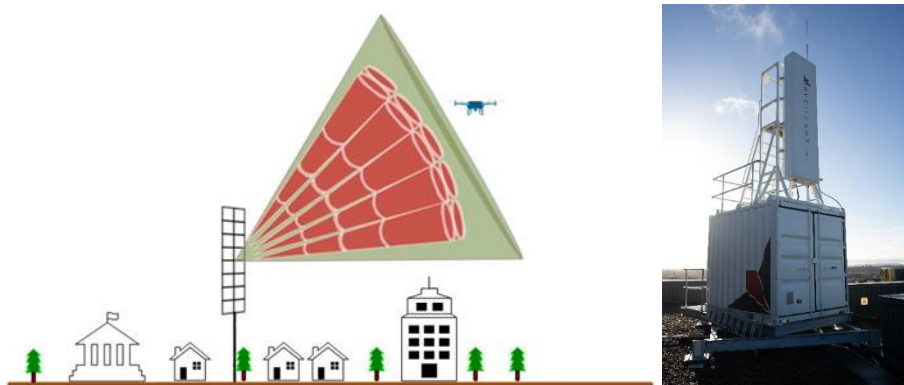

Figure 2: (a) Illustration of the staring radar beam pattern for the single transmitter (green) and multiple receivers (orange) (b) Radar mounted on a cabin that houses the processing rack.

The radar transmits a narrow band unmodulated pulse and the received signal is down converted and matched filtered to record a finite number of range gates per pulse for each receiver channel. The pulses are batched into frames of a fixed number of pulses and the temporal samples from each range bin are coherently integrated. The channel data from each range-Doppler cell is then integrated to generate beamformed range-Doppler data per Coherent Processing Interval (CPI). This provides a 4-D data cube in azimuth x elevation x range x Doppler. This 4-D data can be processed using standard detection techniques to detect and locate moving objects against stationary clutter. The radar produces 3-D detection plots every CPI and after some basic clustering to suppress clutter false alarms, the detections are processed via a Kalman Filter to generate tracks that have position, kinematic and spectral features attributed to each track. The tracker features are further processed via a Bayesian classifier to provide a classification label that is updated every CPI for each track. The real-time process produces classification labels for target categories that comprises drones, birds, ground vehicles and a few other manned aircraft classes. These and other features enable the staring radar to have the necessary sensitivity and Doppler resolution for reliable detection, tracking and classification of drones, birds and other small objects in strong clutter [7] over several kilometre range.

3.2 UOB Networked Staring Radar Testbed

Two staring radars were installed 4 km from Birmingham city centre to operate within a dense urban environment. The choice of location was determined by the underlying principle that detection performance can be limited due to PN, especially close to carrier Doppler frequencies which can impact the signal-to-noise (SNR) for slow-moving targets. PN becomes apparent in the presence of extremely strong clutter and can suppress weaker signals close to zero Doppler. As urban environments have increased instances of strong clutter it is important to establish performance limits within an urban setting and for this reason, the radars are installed on rooftops of buildings at UoB Edgbaston campus in UK. Figure 3 is a Google Earth image with the position of the two radars marked along with their nominal coverage. The insert are images of the respective radar. Radar #1 referred to as GK000 is at a height of 186m and Radar #2 referred to as GK007 is at 176m above mean sea level. The radars are oriented in azimuth so they have overlapping coverage. The relative baseline between the two radars is 180m.

The radar operation is controlled via a custom GUI that also allows quick visualisation of the data during live operations. Additionally, standard tools have been developed for offline processing that are used to benchmark the research outputs. Currently, each radar operates using its own local conventional reference oscillator that is free running with no direct synchronisation between the two radar nodes. The radar can be operated individually as a monostatic system or in a bistatic configuration where one of the radars is transmitting and the other radar is set to receive only mode by setting its transmit power to zero. The receive only radar will provide bistatic data using the other radar as its illuminator of opportunity. In this case, the primary radar is operating as a standard monostatic system that both transmits and receives.

The objective is to obtain benchmark performance results for urban environment with both monostatic and bistatic radar configurations using their conventional oscillators. This provides the basis to repeat measurements with the radar operating with external reference oscillators. The measurements from the radar trials will enable comparative analysis and understanding of the impact of (a) oscillator short term PN on detection sensitivity in high clutter and (b) oscillator longer term stability on network synchronisation.

Figure 3: Coverage map for Radar #1 (yellow) and Radar #2 (purple). Bistatic baseline is 180m.

4.0 RADAR BENCHMARKING

4.1 Field Trials Set-Up

The initial benchmarking trials with the testbed are conducted with the radar using the internal conventional OCXO to provide a baseline against which the alternative external oscillators can be then compared at a later stage. The two radars were set-up as a non-coherent network and this is where one radar operates in its standard configuration so that it is both transmitting and receiving. The second radar is then configured in receive only mode. With two radars there are two alternative network configurations that are possible and Table 1 lists these which are referred to as Network A and Network B respectively.

Table 1: Operational mode of the 2-node non-coherent networked radar.

Item	Unit ID	Operation Mode	Comment
Network A	**GK000**	**Tx and Rx**	**Primary (monostatic) radar**
	GK007	Rx only	Bistatic receive only radar
Network B	GK000	Rx only	Bistatic receive only radar
	GK007	**Tx and Rx**	**Primary (monostatic) radar**

Two measurement campaigns were conducted with the radar, the first one in July 2022 and the second in September 2022. On each occasion, two one-hour live radar missions were performed with each of the two network configurations over the same day. This way monostatic and bistatic data was recorded with each of the two radars providing four separate raw data sets.

For each mission, a number of control flights were performed using different rotary wing drones. The flight paths were specified using waypoints that can be either pre-programmed into the drone or flown manually by an operator on linear paths between waypoints. Figure 4a is a map of the waypoints and the flights are performed at a fixed height, the target is landed between flights and the flight is repeated in both forward and reverse directions. Furthermore, at the specified launch point the flights were performed at a variety of heights and speeds to provide a diverse dataset of target signatures. Figure 4b plots the resultant GPS truth from flights performed with two rotary wing drones at two different altitudes for repeated missions from a single day.

The radar performance is benchmarked by analysing the data both from stationary clutter and the control test flights. The following sub-sections report the analysis firstly for the case of the monostatic measurements and repeated with the bistatic data obtained using the UoB networked testbed.

(a)   (b)

Figure 4: (a) Flight path waypoints plotted as blue lines (b) Drone GPS truth plotted as white lines showing data from multiple flights at two heights

4.2 Monostatic Radar Results

Figure 5 shows a clutter map generated by plotting the zero Doppler signal as a function of range and azimuth at a fixed altitude. The data is scaled for range and the maps are generated using monostatic range-Doppler data from the elevation beams corresponding to the radar height for each of the two radars. The clutter maps are generated by averaging over 512 frames which roughly equates to around 3 minutes of data.
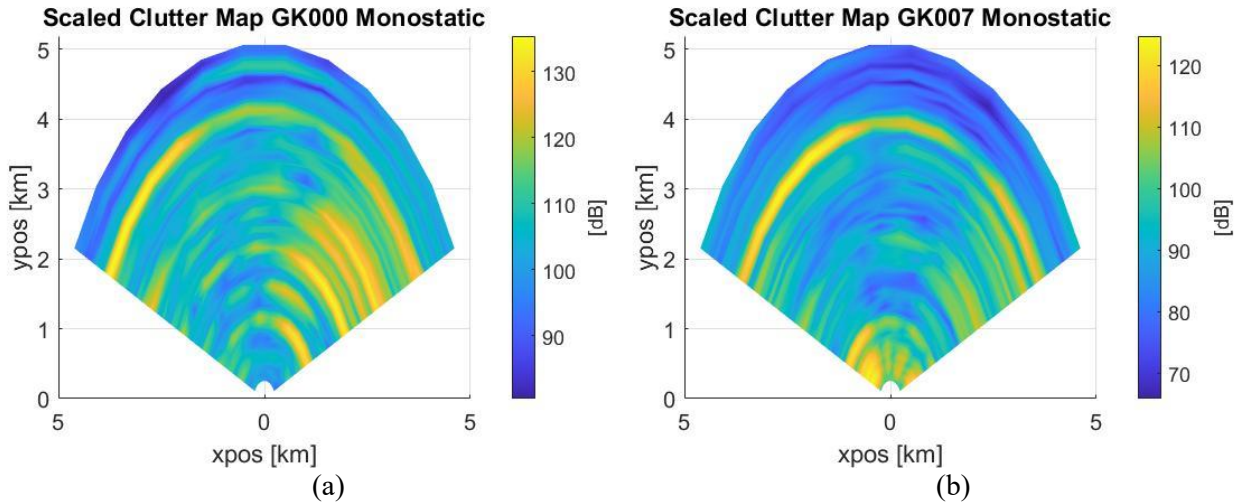

(a)   (b)

Figure 5: Comparison of the monostatic clutter plots at 0Hz Doppler (a) GK000 (b) GK007.

These plots show that there is a much higher level of clutter on the right-hand edges for GK000 which corresponds to high-rise city buildings. There are several other regions of strong clutter that corresponds to the locations of high-rise buildings. There is one particular region of strong clutter a the far left that is visible in both plots. This is a multi-storey office block that is in the line-of-site of both radars and provides a good location for comparative measurements of clutter strengths. The building is photographed in Figure 6a and its relative location with respect to the radar is listed in Table 2. The Doppler return from this strong stationary clutter is quite stable over time and is able to provide an estimate of the radar PN.

PN is measured as relative power to carrier frequency in dBc as a function of Doppler offset. For the received data that is at baseband, this is the ratio with respect to the power at zero Doppler. Thus, in order to compute the PN firstly the mean background power at the specified location is estimated for a range of Doppler frequencies using the same temporal averaging process used to obtain the clutter map. Dividing the measured mean power by the zero Doppler power then gives the PN plot as reported in Figure 6b. This result that compares the two monostatic radars shows that GK000 has a higher PN which implies that the target SNR for this radar is more likely to be clutter limited.

The impact of the radar PN on target signature quality is further examined by comparing the spectrogram of the control drone (detailed in Table 3) and analysing the target signature characteristics from each radar. The target spectrogram is generated by using the GPS truth data to specify the range and beam location for each CPI frame and extracting the Doppler profile from the 4-D azimuth x elevation x range x Doppler data and concatenating these over multiple frames. In the spectrogram, static clutter appears at zero-Doppler and the target body Doppler will appear offset from the clutter for non-zero radial velocities. Figure 7 compares the spectrogram obtained with each radar for I3-D drone that flew the same pattern clockwise at a constant height of 100 m above ground. Note that both the drone body echo and the micro-Doppler returns from the drone rotor blades are more visible in GK007. This is in part due to GK007 having a higher transmit power. However, what is also noticeable is that in GK000, data between timeframe 300 to 500, the background level is raised which is suppressing the target echoes. This raised background is as a result of PN in the presence of high clutter. This is consistent with the result reported in Figure 6b which recorded GK000 to have a higher PN.

Table 2: Location information of a multi-storey block visible in the clutter map of both radar

Location	GK000 Range Gate	GK000 Azimuth [deg]	GK000 Elevation [deg]	GK007 Range Gate	GK007 Azimuth [deg]	GK000 Elevation [deg]
Multi-storey block	50	148	90	48	136	90

| (a) | (b) |
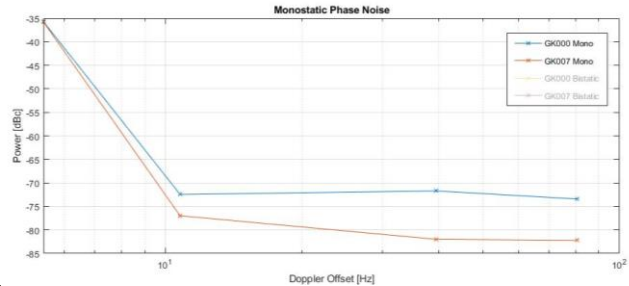
Figure 6: (a) Photograph of the multi-storey block (b) Monostatic PN measured at the selected location.

This impact of higher clutter on the noise background is further evident in the corresponding plot comparing the clutter, target and mean noise power that are derived from the target spectrogram data. From the results plotted in Figure 8, it is evident that the noise floor in GK000 is raised for timeframes that report a higher clutter power. This is where the PN of the radar is causing the background to become clutter limited. In comparison, the noise lower in GK007 is lower and remains so irrespective of the clutter power implying that the background is at thermal noise power which is consistent with the system having a lower PN. Incidentally, Figure 8 is also showing a higher target power for GK007 which is consistent with the system operating at a higher transmit power.

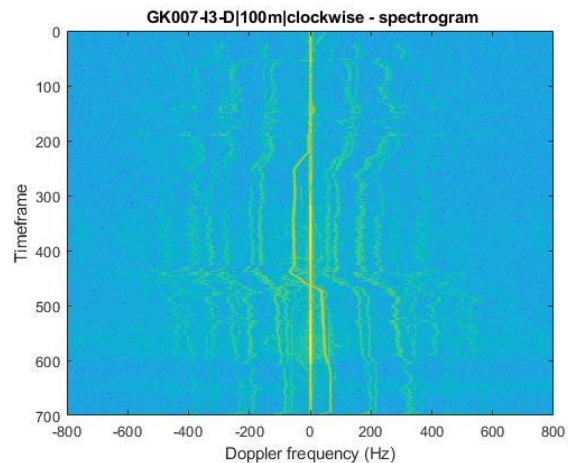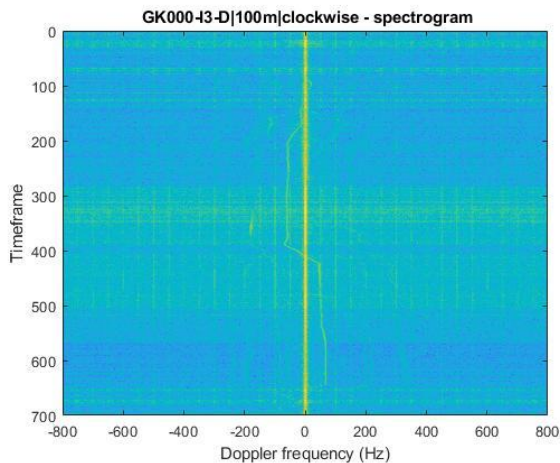| Name	Target ID	Description	Image
DJI Inspire 2	I3-D	4 rotor medium size drone	

| (a) | (b) |

Figure 7: Monostatic spectrogram of I3-D from clockwise flight at 100m height (a) GK000 (b) GK007.
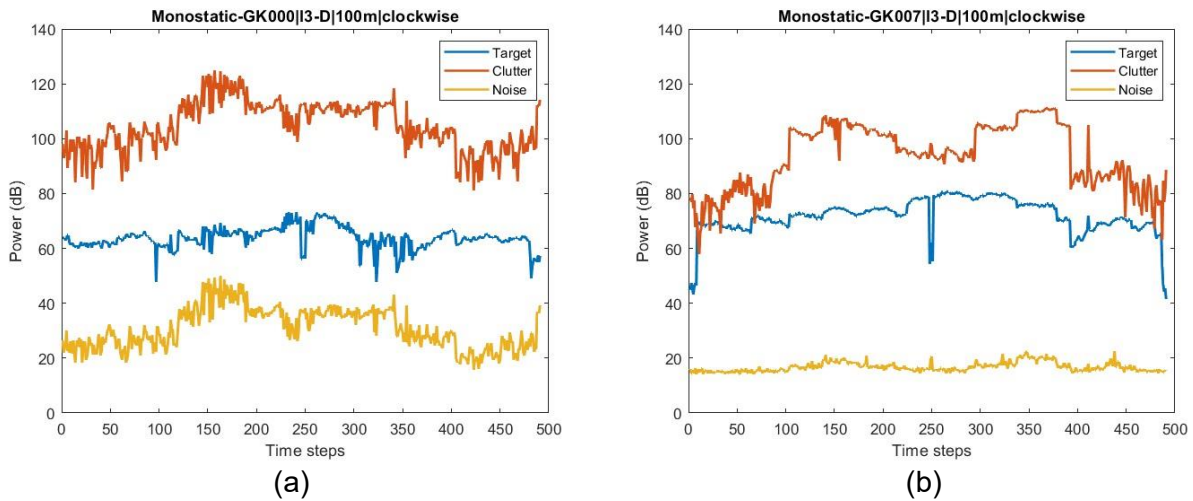
Figure 8: Monostatic result for I3-D target power, clutter power and mean noise power (a) GK000 (b) GK007.

4.3 Bistatic Radar Results

The processing steps for generating the clutter map and target spectrogram from the bistatic measurements are exactly identical to that used with the monostatic data except for one crucial difference. Due to the lack of synchronisation in the non-coherent network, the bistatic data has to be corrected for Doppler offset due to clock drift and range misalignment as a result of timing offset in the pulse trigger. A software based method was implemented that uses the direct signal to estimate both of these offsets and correct the raw data. Reference [8] provides full details of the software based method for correcting the non-coherent data and this was applied to the radar data prior to generating the bistatic clutter maps and target spectrogram data.

Figure 9 compares the bistatic clutter map and these are more similar between the two radars compared to the equivalent monostatic clutter maps (see Figure 5). This is because the combined bistatic coverage map is very similar and therefore the corresponding clutter maps are more alike. Figure 10 is the corresponding bistatic PN measured for the same location as listed in Table 2. Again this reflects a combination of the PN between the transmit and receive system and the values are closer between the two radars and overall the PN is higher than the monostatic radar. This is again expected as there is no self-cancellation of PN in the bistatic configuration which leads to a higher PN.
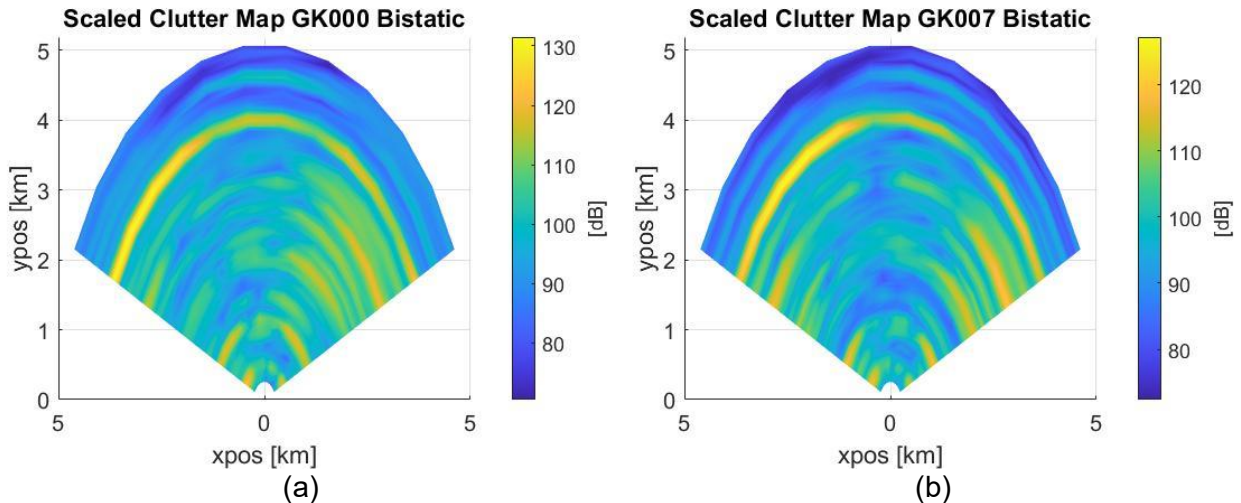

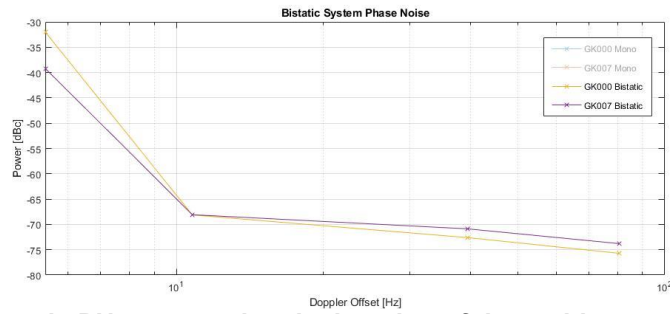**Figure 9: Comparison of the bistatic clutter plots at 0Hz Doppler (a) GK000 (b) GK007.**

Figure 10 :Bistatic PN measured at the location of the multi-storey block listed in Table 3.
This higher PN is also evident in the target spectrogram of the bistatic data (Figure 11) from the same flight for which monostatic plots were shown earlier. Note for example for GK007 for timeframes 300 to 350 in Figure 11b the background level is raised whereas previously GK007 data was on the whole noise limited for this flight. The same trends can be observed in the plot shown in Figure 12 where the overall noise floor level is higher even though the bistatic clutter power is lower compared to the equivalent monostatic values. This confirms that the PN in the bistatic measurements are higher compared to the monostatic values and is in line with that reported in Figure 10 which was estimated using the strong clutter reference point.
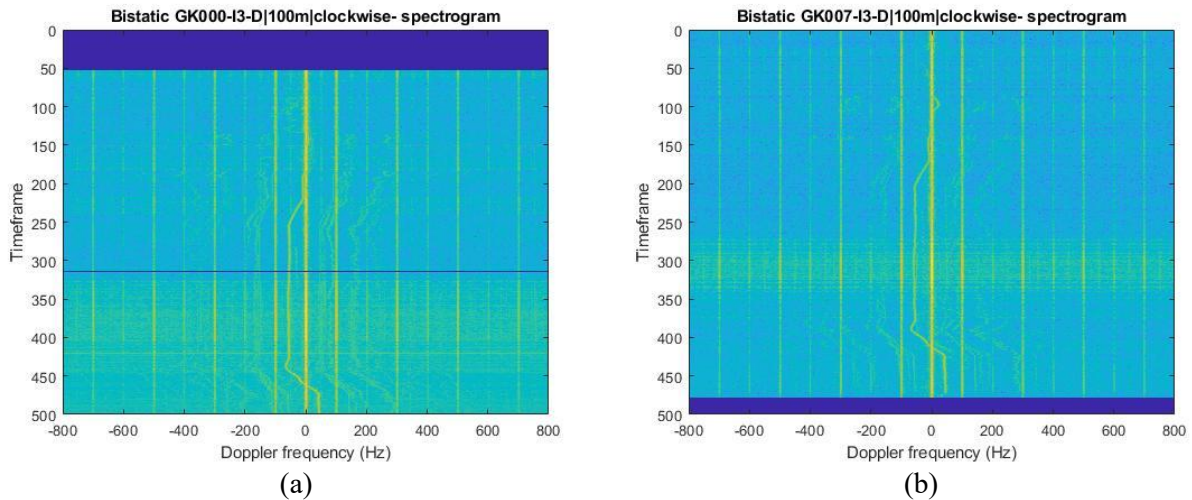

(a)   (b)

Figure 11: Bistatic spectrogram of I3-D from clockwise flight at 100m height (a) GK000. (b) GK007
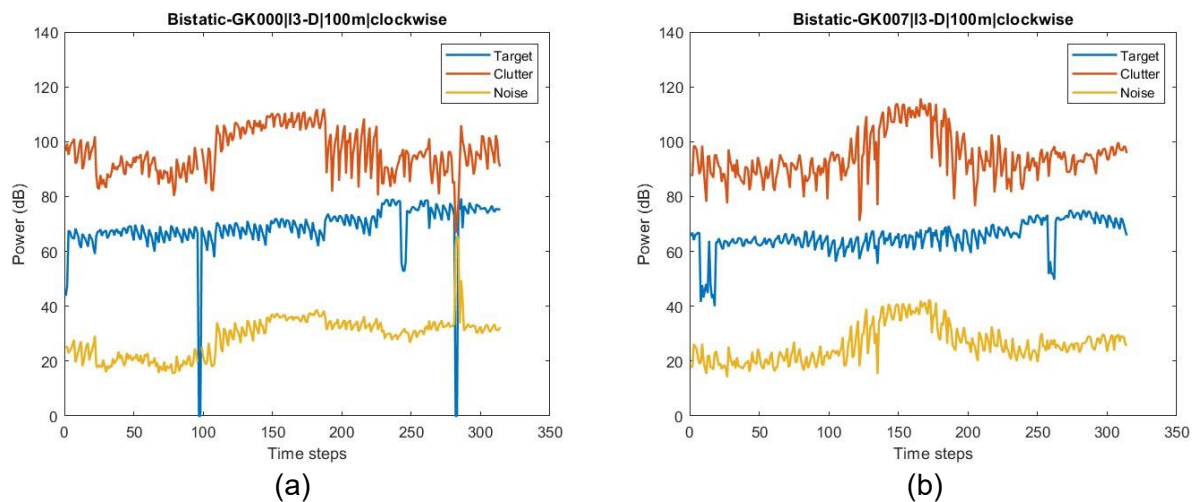

(a)   (b)

Figure 12: Bistatic result for I3-D target power, clutter power and mean noise power (a) GK000 (b) GK007.

5.0 OSCILLATOR BENCHMARKING

5.1 Bench Test Set-Up

The bench tests are performed to characterise the Oscillator Under Test (OUT) on their own and also when connecting to the radar. The staring radar front-end uses a Phase Locked Oscillator (PLO) that has a conventional OCXO that provides the RF Local Oscillator (RF_{LO}) that then derives a Timing and Waveform Generation (TWG) board that up converts it to the RF Carrier waveform (RF_C) and the pulsed output is used for transmission. The external oscillator is used to provide the Reference Oscillator (RF_{RO}) that can either lock the PLO or input directly to the TWG. Figure 13 illustrates the schematic of the interface and for the bench test, the OUT was always connected directly to the TWG that then bypasses the PLO. The primary FoM is the PN which is measured at both the OUT reference frequency (Probe B) and at the output of the TWG (Probe C) which is the upconverted RF. The former provides a measure of the source PN of the OUT and the latter an understanding of the transmit waveform PN when it is being referenced to the OUT. PN is a measure of the short term stability and is useful in assessing the detection sensitivity in presence of strong clutter. It is specified in units of dBc/Hz and the measurements are performed using a Rohde & Schwarz Phase Noise Analyser.
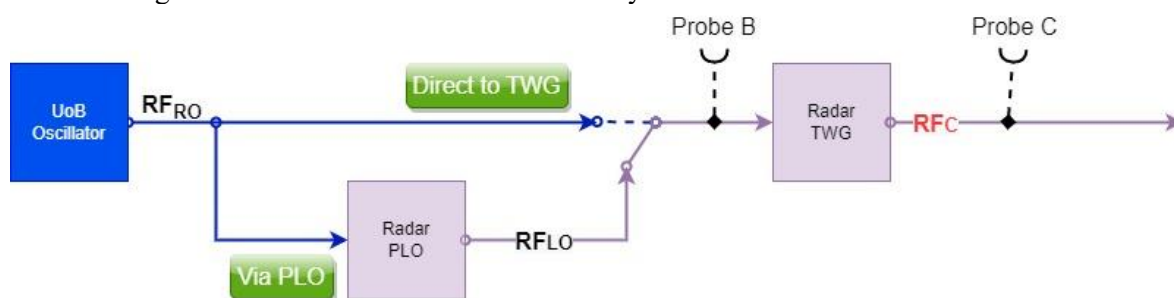

Figure 13: Schematic of the radar front-end interface with OUT.

For synchronisation, the relative stability of the pair of OUTs is measured using the overlapping Allan Deviation (AD). The bench tests are carried out by connecting each pair of OUTs to the input channels of K+K Frequency Counter which is referenced to a 10 MHz external source (Figure 14). The frequency ratio measured with the counter is used to compute the overlapping AD.
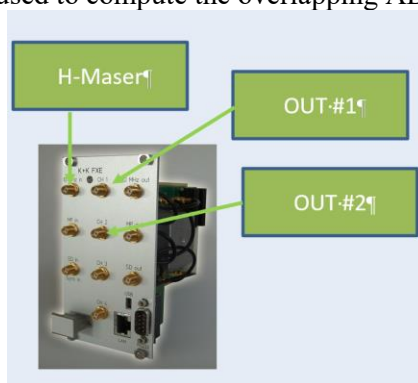

Figure 14: Measurement set-up for overlapping AD with two OUTs using the K+K FXE frequency counter.

5.2 Phase Noise Results

The test results were obtained for (i) Radar PLO (ii) Menlo and (iii) GPS Disciplined Oscillator (GPSDO). The bench test (Figure 15) shows that compared to the radar PLO, the PN for Menlo is considerably lower at low Doppler offset frequencies whereas at higher frequencies the conventional OCXO does perform better. Note that the difference is less at the TWG output where the frequencies are up converted but the overall trend is for the Menlo to show a 5-10 dB improvement at 10Hz offset. Results for GPSDO are also included although it uses a TCXO oscillator and has worse PN across all frequencies.
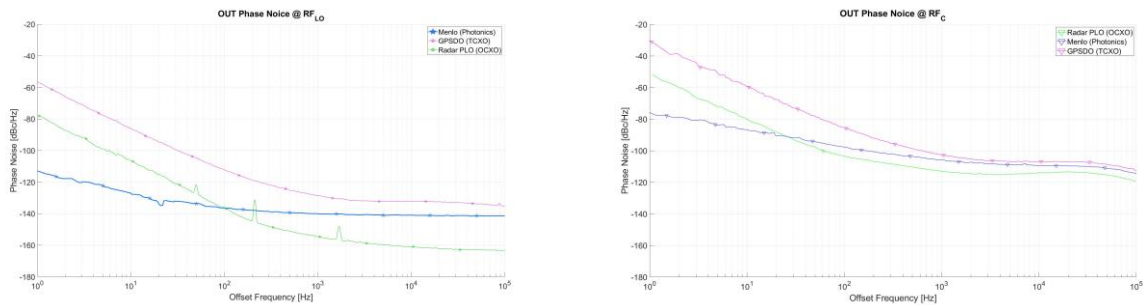
Figure 15: Bench test PN measurements for Menlo, GPSDO and Radar PLO (a) RF$_{LO}$ (b) RF$_C$.

5.3 Allan Deviation Results

Figure 16 compares the overlapping AD using pairs of oscillators. In each case, the same OUT used for the PN measurements were used apart from the radar PLO where the actual OCXO used within the PLO were tested. The GPSDO that is locked to the GPS satellite does show a marked improvement on the free running OCXO but the Menlo has a far better AD. Here each of the Menlo OUT were free running and the RF output were being disciplined by its own internal ORS. The level of frequency stability reported for Menlo will be very advantageous in network synchronisation.
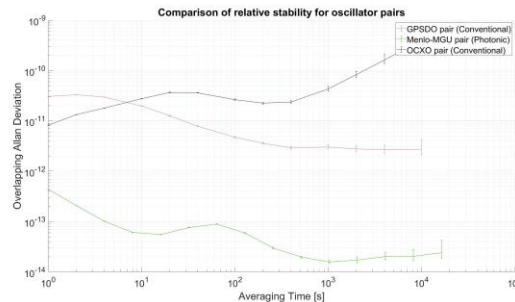

Figure 16: Overlapping AD measured for different oscillators from bench tests.

6.0 IMPLEMENTATION PLAN FOR QUANTUM-ENABLED NETWORKED RADAR

Both of the staring radars have been upgraded to have the new interface board installed that enables connectivity to the external reference oscillator. The first of the two Menlo have been installed in one of the radar cabins (Figure 17) and its been commissioned. Connection to the radar TWG that is housed in the radar radome mounted on the cabin roof will be through a 15m long RF cable. Connection to other components of the Quantum oscillators that are housed in a lab in an adjacent building is via a comms fibre link and these other sub-systems will come on-line at a later stage. The second Menlo will be also installed in the other radar cabin by end of spring 2023. The test will be repeated with three oscillators (i) The radar PLO that has an OCXO (ii) the GPSDO that uses a TCXO and (iii) the Menlo that uses an F-Comb locked to a local ORS. In each case the PN at the output transmit frequency will be measured and raw radar data will be collected that will include repeating the control drone flights. Initial measurements will be carried out with each radar operating monostatically and this will then be repeated with the bistatic network configurations.

The range-Doppler data will be analysed, and comparison will be made of the PN estimated on strong clutter similar to the processed used for radar benchmarking. Data from the control drone flights will be used to quantify the SNR as a function of the reference oscillator. A full comparison of the monostatic and bistatic radar performance in realistic urban clutter for small targets using different oscillators including the photonics device will inform on the utility of ultra low PN in surveillance radar and networked sensors.

Figure 17: First of two Menlo systems set-up in the UoB staring radar testbed.

7.0 SUMMARY

Significant development has taken place toward setting up a Quantum-enabled networked staring radar testbed. A blue print has been provided for assembling a quantum oscillator and the PN and longer term stability of the Menlo photonics oscillator has been compared with conventional radar oscillator using bench tests. A networked staring radar testbed has been set-up in an urban environment to provide real world evaluation of high performance oscillators against existing radar technology. Benchmark results are obtained from live radar trials to provide a baseline to compare performance against a range of alternative oscillators. The testbed is now fully configured to be able to take local oscillator from an external reference and a full set of measurements are due to commence to evaluate detection sensitivity and network synchronisation against photonics oscillators and their Quantum variants.

8.0 REFERENCES

[1]   Menlo Systems GmbH, "PMWG 1500 product web page," [Online]. Available: *https://www.menlosystems.com/products/ultrastable-microwaves/pmwg-1500/*. [Accessed Mar 2023]

[2]   Bradler M, *et al.*, Photonic Microwave Generator as Quantum Local Oscillator for Radars, *2022 Joint Conf. Europ. Freq. & Time Forum and IEEE Intern. Freq. Control Symposium*, Paris, France, Apr. 2022

[3]   Xie X *et al.,* Photonic microwave signals with zeptosecond-level absolute timing noise , *Nature Photonics*, vol. 11, no. 1, pp. 44-47, 2017

[4]   Jahangir M, Jones J M, *et al.*, Development of Quantum Enabled Staring Radar with Low Phase Noise, EuRAD 2021, London, Apr 2022

[5]   Jahangir M, Baker C J, *et al.*, Doppler characteristics of micro-drones with L-band multibeam staring radar, *IEEE RadarCon 2017*, Seattle, US, May 2017

[6]   Jahangir M, Target centric wide-area 3-D surveillance using a non-scanning multibeam receiver array, *IEEE Radar 2015*, US, May 2015, pp. 652-7

[7]   Jahangir M, and Baker C J, L-band staring radar performance against micro-drones, *IRS 2018*, Bonn, Germany, Jun. 2018

[8]   Griffiths D, Jahangir M, *et al.*, Direct Signal Synchronization for staring Passive Bi-static Radar, IET Radar Conference 2022, Oct 2022